ELSEVIER

Light-induced ultrafast proton-coupled electron transfer responsible for H_2 evolution on silver plasmonics

Yocefu Hattori [1], Mohamed Abdellah [1,2,*], Igor Rocha [3], Mariia V. Pavliuk [1], Daniel L.A. Fernandes [1], Jacinto Sá [1,4,*]

[1] Department of Chemistry, Ångström Laboratory, Uppsala University, 75120 Uppsala, Sweden
[2] Department of Chemistry, Qena Faculty of Science, South Valley University, 83523 Qena, Egypt
[3] Department of Engineering Sciences, Ångström Laboratory, Uppsala University, 75121 Uppsala, Sweden
[4] Institute of Physical Chemistry, Polish Academy of Sciences, 01-224 Warsaw, Poland

Light-driven proton-coupled electron transfer (PCET) reactions on nanoplasmonics would bring temporal control of their reactive pathways, in particular, prolong their charge separation state. Using a silver nano-hybrid plasmonic structure, we observed that optical excitation of Ag-localized surface plasmon instigated electron injection into TiO_2 conduction band and oxidation of isopropanol alcoholic functionality. Femtosecond transient infrared absorption studies show that electron transfer from Ag to TiO_2 occurs in ca. 650 fs, while IPA molecules near the Ag surface undergo an ultrafast bidirectional PCET step within 400 fs. Our work demonstrates that ultrafast PCET reaction plays a determinant role in prolonging charge separation state, providing an innovative strategy for visible-light photocatalysis with plasmonic nanostructures.

Introduction

Proton-coupled electron transfer (PCET) is quintessential for a plethora of energy conservation processes in chemistry and biology and the prime enabler for kinetically competent multielectron redox transformations [1–6]. The most celebrated PCET reaction is the catalytic water oxidation that involves the transfer of $4e^-/4H^+$, which is masterfully executed by the photosystem II [7,8]. Photo-induced PCET offers an almost barrier-less reaction pathway to govern reactions toward desired products. The process operates via concerted or sequential steps of electron transfer (ET) and proton transfer (PT) [9–12].

The present examples of photo-induced PCET tend to exploit the long-lived triplet state of molecular dyes to prompt the competition between PCET steps and undesirable deactivation processes [11,13], Schrauben et al. demonstrated the universal character and importance of PCET in chemical energy technologies driven reactions by reporting its occurrence in metal oxide nanoparticles, such as TiO_2 and ZnO [14].

Although most of the reported PCET cases occur in the kinetic domain (time scale of ns and above), there are a few man-made examples operating in the ultrafast domain, in which the entire process occurs within a few picoseconds. The most notorious is the concerted ET–PT process through an intramolecular charge-transfer excitation of a hydrogen-bonded paranitrophenyl-phenol:tert-butylamine pair reported by Westlake et al. [10], which is able to perform the entire process within 200 fs. Additional systems have been proposed elaborating on the Westlake et al. strategy, such as the octahedral Pd_6L_4 molecular cage by Gera et al. [15] capable of concerted ET–PT steps within 900 fs.

Gold group metallic nanoparticles (NPs) exhibit large optical cross-sections in the visible domain related to the excitation of localized surface plasmons (LSP), making them highly attractive for chemical energy reactions. However, their direct application is limited due to LSP short lifetime. LSP excitation creates a non-Fermi distribution of electrons that rapidly relaxes to a Fermi distribution via electron–electron (e–e) scattering, with

* Corresponding authors at: Department of Chemistry, Ångström Laboratory, Uppsala University, 75120 Uppsala, Sweden.
E-mail addresses: Abdellah, M. (mohamed.qenawy@kemi.uu.se), Sá, J. (jacinto.sa@kemi.uu.se).

https://doi.org/10.1016/j.mattod.2018.05.002

relaxation dynamics dependent on induced transition (intra- or interband transition). For Ag (stronger absorber) excitations occur through the plasmon resonance yielding electrons with energies between 0 and 3.2 eV above the Fermi level. This equates to e–e scattering time of ca. 8 fs (at the average electron energy of 1.6 eV) [16] making it impracticable for photocatalysis. For further information on plasmonics and hot carriers dynamics, we recommend the following reviews [17–21].

Recently, we proposed a silver nano-hybrid architecture fabricated via a modular bottom-up synthesis approach capable of attaining a long-lived charge separated state upon visible light excitation and consequently concomitantly catalyze proton reduction and pollutant oxidation at record levels [22], firmly supporting plasmonic nanostructures as a key approach to produce solar a fuels, a process recently listed among the 2017 top 10 emerging technologies by the World Economic Forum.

The blueprint of the nano-hybrid system consisted of Ag NPs stabilized by betanin, a molecular linker, TiO_2 as a semiconductor and Ru NPs as H_2 evolution co-catalyst. The molecular linker (4-aminobenzoic acid, pABA) linked the Ag to TiO_2 improving the electronic coupling between donor and acceptor units, which enabled ultrafast (ca. 800 fs) and effective electron transfer between units. One might expect that the good electronic connectivity between the two units should also intensify the undesired recombination pathway, which did not occur. Hence, a stabilization mechanism was suspected to be taking place, at the time, with betanin units believed to play a preponderant role.

This work aims to show that indeed a stabilization mechanism is accountable for the long-lived charge-separated state in silver nano-hybrid architecture and that PCET is the responsible process for the increase in charge separation lifetime. To ascertain this claim, a self-assembled nano-hybrid architecture composed of polyvinylpyrrolidone (PVP)-stabilized Ag NPs (average size SEM = 19 ± 7 nm, DLS = 36 ± 10 nm) molecularly linked to TiO_2 anatase (average size ca. 25 nm) with pABA was synthesized. By replacing betanin with PVP, the potential PCET functionality in the original system is removed, and PCET process is restricted to solvent molecules. In the present case, isopropanol (IPA) was used as solvent and as bidirectional PCET agent (Fig. 1) [23]. Femtosecond transient infrared absorption spectroscopy (TIRAS) was used to monitor simultaneously the PCET on IPA and electron injection into TiO_2 CB. Details on experimental procedures and standard sample characterization can be found in Supporting information.

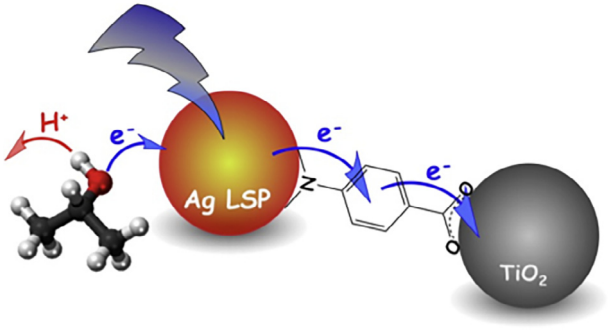

FIGURE 1

Conceptual representation of Ag nano-hybrid system and photoinduced bidirectional PCET process.

Experimental

Ag NPs synthesis

Silver nitrate (Sigma–Aldrich, ≥99%) was the metal precursor for the synthesis. $NaBH_4$ and NaOH (Fluka Chemical, ≥99%) were used as the reducing agent, while polyvinylpyrrolidone (PVP, Sigma–Aldrich, m_w = 10000) and ethylene glycol (Fluka Chemical, ≥99.5%) as the stabilizing agent and dispersing agent, respectively. All the compounds were dissolved in distilled water through the use of a magnetic stirring bar followed by 10 min of sonication in the ultrasonic cleaner (EMGA Emmi-05P). The steps for the synthesis of the Ag nanoparticles were mostly based on work of Ajitha et al. [24].

After the synthesis, the PVP Ag nanoparticles were precipitated by adding acetone (VWR Scientific ≥99%) and centrifuging for 1 min in a rotational speed corresponding to 1000*g*. The supernatant was removed, while the remaining precipitated was dried with argon gas. Subsequently, the Ag nanoparticles were dispersed by adding isopropanol (EMSURE ≥99.8%) and sonicated for 10 min. A second centrifugation for 25 min in 2500*g* was then applied in order to remove particles bigger than ≈ 50 nm.

Nano-hybrid sample preparation

Titania 18NR-T transparent paste was purchased from Greatcellsolar with average nanoparticles size of 25 nm. A simple Doctor Blade (or tape casting) technique was applied to produce thin film of TiO_2 over a CaF_2 glass and put thereafter in an oven, which was heated until 500 °C with predetermined changing rate. The CaF_2 window with the titania was then immersed in a solution of 3.6 mM of 4-aminobenzoic acid (Sigma–Aldrich, >99%) in isopropanol for approximately 1 h. The solution of Ag nanoparticles was finally dropped over the functionalized titania film, and the sample was mounted in a Harrick flow cell.

Femtosecond transient infrared absorption spectroscopy (TIRAS)

The 1 mJ, 45 fs output of a 1 kHz Ti:Sapphire amplifier (Spitfire Pro, Spectra-Physics) was split into two separate commercial optical para-metric amplifiers (TOPAS-C, Light Conversion), which generate the visible pump 430 nm and the mid-IR probe (1100–1250 cm^{-1}) pulses. Prior to reaching the sample, the probe beam was split into equal intensity probe and reference beams using a wedged ZnSe window. Both beams pass through the sample, but only the probe beam interacts with the photo-excited volume of the sample. All beams are focused with a single f = 10 cm off axis parabolic mirror to a ~70 μm spot size in the sample. The pump intensity was set to c.a. 300 μW. The probe and reference beams were dispersed by a commercial monochromator (Triax 190, HORIBA Jobin Yvon) equipped with a 75 groove/mm grating and detected on a dual array, 2 × 64 pixel mercury cadmium telluride detector (InfraRed Associated, Inc). The instrument response function for the experiments was approximately 200 fs. The same equipment has been constantly used previously for other experiments [22].

Results and discussion

Standard characterization of the Ag NPs and spectroscopic evidences confirming linkage of Ag NPs to TiO_2 via the molecular linker can be found in Supporting information. Fig. 2 shows the temporal evolution of the TIRAS signal upon excitation at 430 nm. The wavelength was selected to restrict sample excitation to silver plasmon resonance. The transient signal is dominated by a broad absorption and two bleach peaks at 1160 and 1128 cm^{-1}. The bleach signals appear to overlap with the peaks attributed to the C–O stretching of the IPA alcoholic functionality [25], suggestive of C–OH oxidation (IPA oxidation potential onset on Pt electrode is 0.25 V vs SCE both in acid [26] and alkaline [27] conditions). Note, that the observed changes in the C–O stretching are not associated with carboxylic group of the linker because the carboxylic group is present in all experiments with linked system, but the signal change was only observed when IPA is present. Additionally, the signal is located at lower frequency that the one expected for an acid C–O stretching, which appears at 1210–1320 cm^{-1} [28]. The positive absorption is ascribed to electrons in the TiO_2 CB [22,29]. Free electrons in the CB yield a characteristic strong and broad absorption across the entire infrared domain originated from the quasi-metal state formed as soon as the electrons are injected into the semiconductor CB [29]. The signal is also present in the bleach region but difficult to visualize due to the overlap with the bleach peaks that have a higher extinction coefficient [25,30].

To establish the processes, kinetics traces for the electrons in TiO_2 CB (average signal between 1222 and 1227 cm^{-1}) and IPA C–O stretching bleach (average signal between 1157 and 1161 cm^{-1}) were extracted from Fig. 2. The results are presented in Fig. 3. Since the raw bleach signal has a positive contribution from electrons in TiO_2 CB, post-treatment of the signal was needed. By fitting each infrared spectrum with the Drude model [31,32], and subsequently subtracting this contribution to the bleach intensity, enabled effective removal of the electrons in TiO_2 CB contribution to the bleach signal. Details about the Drude model can be found in Supporting information. Both kinetic traces have a distinct rising edge component, which are larger than the instrument response time ca. 200 fs. The rising component for the bleach signal is 400 fs and provides information of the time necessary for the bidirectional ultrafast PCET step to take place, which is faster than the time scale for bulk solvation [15]. At 400 fs, this is among the fastest ever recorded PCET event [10,15]. The rising component for electrons in TiO_2 CB is slightly longer (ca. 650 fs), and yields the time necessary for electrons to travel from Ag to the TiO_2 via the molecular linker.

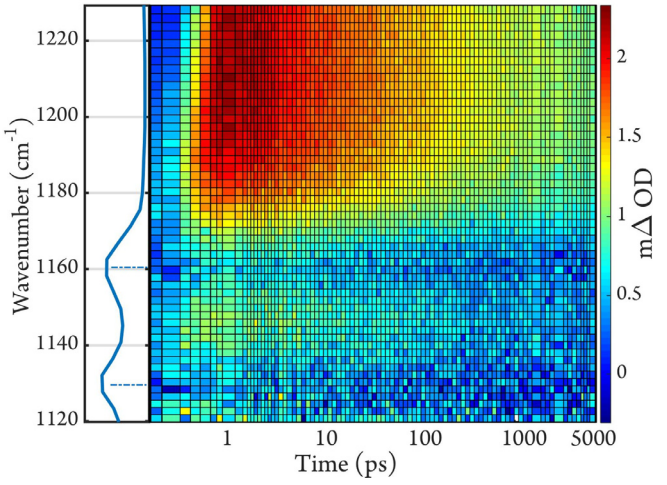

FIGURE 2

Temporal evolution of the ultrafast infrared absorption spectra upon excitation at 430 nm. Side banner shows the Fourier-transformed infrared spectrum of neat IPA.

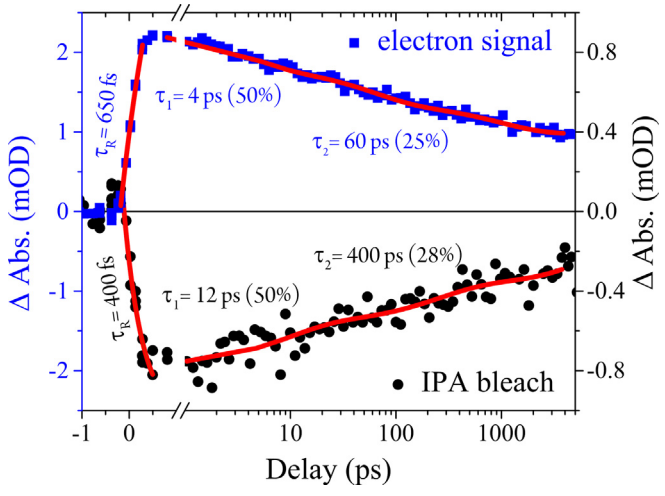

FIGURE 3

Kinetic traces and fittings for (top panel) electrons in TiO_2 CB and (bottom panel) IPA bleach due to oxidation after subtraction of the electrons in TiO_2 CB contribution.

Apart of the rising edge, the kinetic traces were also fitted with three exponential decay components. The simple fact that the signals decay confirms the reversibility of the process. Hence, the IPA bleach is related to one-electron oxidation of the alcoholic functionality not two electrons, i.e., oxidation of C–OH to C–$O^{\bullet -}$. Thus, IPA donates one electron to Ag to quench its reactive hole and transfers a proton to a separate base, in this case OH^- and/or water present in the solvent. The longest decay component for electrons in TiO_2 CB with time constant 1.1 ns accounting to roughly 25% (Fig. 4) is symptomatic of a stabilization mechanism and paramount for the effective utilization of sensitizers with lifetimes in the 10 s of fs [16] in photocatalysis [22].

To establish that PCET process is the culpable for the prolonging of the charge separation state in the Ag nano-hybrid plasmonic architecture, similar experiments were performed in dry films, i.e., in the absence of a PCET agent (IPA). The effect on the electrons in TiO_2 CB signal is plotted in Fig. 4 against the experiment in the presence of IPA. The rising edge components are not too dissimilar, suggesting that electron-traveling time from Ag to TiO_2 is not significantly affected by the absence PCET agent. The same cannot be said for the decay components. It is clear that in dry films electrons in TiO_2 CB decay significantly faster than in the presence of IPA. In the dry films electron-hole recombination occurs in less than 500 ps making it inapt for photocatalysis. This contrast with the case where IPA is

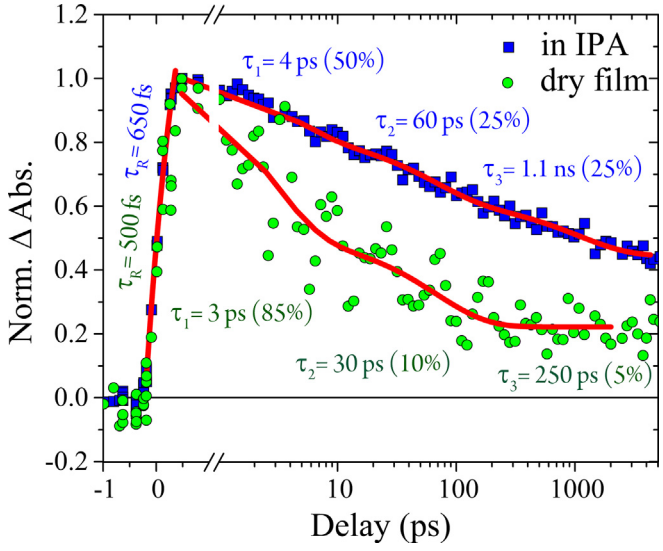

FIGURE 4

Decay kinetics at related to electrons in TiO_2 CB for dry film and in IPA.

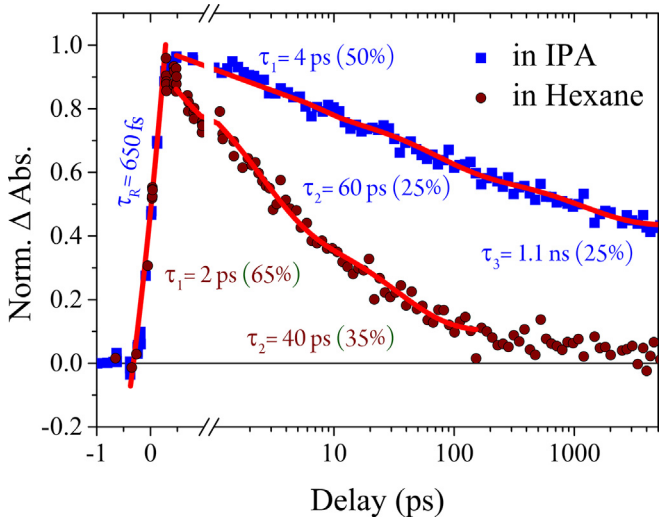

FIGURE 5

Decay kinetics at related to electrons in TiO_2 CB in IPA and hexane.

present and PCET is taking place, which causes the formation of a charge separated state beyond nanoseconds. The observation is consistent with the hypothesis that PCET is the responsible mechanism for charge separation stabilization. Similar results were obtained when IPA was replaced by a non-PCET agent, namely hexane (Fig. 5). The result suggests that the reaction medium contributes very little for the observed stabilization mechanism, and thus stabilization is due to PCET event.

Conclusion

In conclusion, we established that an ultrafast PCET process occurs on Ag nano-hybrid plasmonic architecture. The PCET process occurs within 400 fs, making it among the fastest ever recorded [10,15] but more importantly it is the culpable for the stabilization of charge separation state, enabling the system to act as an active photocatalytic system. The presented paradigm for prolonging the charge separation lifetime can be generalized to other short-lived photosensitizers. Furthermore, the paradigm enables us to unlock the potential of the strongest solar light absorbing material, hinder till now due to short lifetime of its excited state.

Author contributions

J.S. proposed the concept and directed the research. Y.H. and M. A. designed the experiments. Y.H, M.A., I.R. and D.L.A.F. carried out the experiments. Y.H. and M.A. prepared the figures. J.S. wrote the main manuscript text. All authors reviewed the manuscript.

Acknowledgments

The authors would like to thank Uppsala University (starting grant), Swedish Research Council (grant no. 2015-03764) and Stiftelsen Olle Engkvist Byggmästare (grant no. 2016/367) for financial support. The authors would like to thank Shmector.com for Fig. 1 background permission. The authors declare no competing financial interest.

Appendix A. Supplementary data

Supplementary data associated with this article can be found, in the online version, at https://doi.org/10.1016/j.mattod.2018.05.002.

References

[1] R.I. Cukier, D.G. Nocera, Annu. Rev. Phys. Chem. 49 (1998) 337–369.
[2] J.M. Mayer, Annu. Rev. Phys. Chem. 55 (2004) 363–390.
[3] M.H.V. Huynh, T.J. Meyer, Chem. Rev. 107 (2007) 5004–5064.
[4] S. Hammes-Schiffer, Acc. Chem. Res. 42 (2009) 1881–1889.
[5] S. Hammes-Schiffer, A.A. Stuchebrukhov, Chem. Rev. 110 (2010) 6939–6960.
[6] C. Costentin, M. Robert, J.-M. Saveánt, Acc. Chem. Res. 43 (2010) 1019–1029.
[7] S. Mukhopadhyay et al., Chem. Rev. 104 (2004) 3981–4026.
[8] J.P. McEvoy, G.W. Brudvig, Chem. Rev. 106 (2006) 4455–4483.
[9] S. Hammes-Schiffer, Proc. Natl. Acad. Sci. USA 108 (2011) 8554–8558.
[10] C.B. Westlake et al., Proc. Natl. Acad. Sci. USA 108 (2011) 8531–8532.
[11] O.S. Wenger, Acc. Chem. Res. 46 (2013) 1517–1526.
[12] T.T. Eisenhart, J.L. Dempsey, J. Am. Chem. Soc. 136 (2014) 12221–12224.
[13] C. Bronner, O.S. Wenger, J. Phys. Chem. Lett. 3 (2012) 70–74.
[14] J.N. Schrauben et al., Science 336 (2012) 1298–1301.
[15] R. Gera et al., J. Am. Chem. Soc. 136 (2014) 15909–15912.
[16] J.H. Hodak, I. Martini, G.V. Hartland, J. Phys. Chem. B 102 (1998) 6957–6958.
[17] M.L. Brongersma, N.J. Halas, P. Nordlander, Nat. Nanotechnol. 10 (2015) 25–34.
[18] S. Linic, P. Christopher, D.B. Ingram, Nat. Mater. 10 (2011) 911–921.
[19] P. Christopher, M. Moskovits, Ann. Rev. Phys. Chem. 68 (2017) 379–398.
[20] S. Tan et al., Nat. Photon. 11 (2017) 806–812.
[21] S. Tan et al., J. Am. Chem. Soc. 139 (2017) 6160–6168.
[22] M.V. Pavliuk et al., Sci. Rep. 7 (2017) 8670.
[23] J. Nomrowski, O.S. Wenger, Inorg. Chem. 54 (2015) 3680–3687.
[24] B. Ajitha et al., RSC Adv. 6 (2016) 36171–36179.
[25] E. Sani, A. Dell'Oro, Opt. Mater. 60 (2016) 137–141.
[26] S.-G. Sun, D.-F. Yang, Z.-W. Tian, J. Electroanal. Chem. 289 (1990) 177–187.
[27] T. Okanishi et al., Phys. Chem. Chem. Phys. 18 (2016) 10109–10115.
[28] http://www2.ups.edu/faculty/hanson/Spectroscopy/IR/IRfrequencies.html.
[29] L.J. Antila et al., Chem. Commun. 51 (2015) 10914–10916.
[30] J.S. Sanghera et al., Appl. Opt. 33 (1994) 6315–6322.
[31] J. Sá et al., Analyst 138 (2013) 1966–1970.
[32] P. Friedli, H. Sigg, J. Sá, Photochem. Photobiol. Sci. 13 (2014) 1393–1396.